Journal of Nuclear Medicine, published on July 28, 2016 as doi:10.2967/jnumed.116.175539

Count rate characteristics and image distortion in preclinical PET systems during intratherapeutic radiopharmaceutical therapy imaging

Emma Mellhammar[1], Magnus Dahlbom[2], Johan Axelsson[3], and Sven-Erik Strand[1,4]

Affiliation*:* [1]Lund University, Department of Clinical Sciences Lund, Oncology and Pathology, Lund, Sweden; [2]Department of Molecular and Medical Pharmacology, David Geffen School of Medicine at UCLA, Los Angeles, CA, USA; [3]Department of Physics, LTH, Lund Sweden; and [4]Lund University, Department of Clinical Sciences Lund, Medical Radiation Physics, Lund, Sweden

Disclaimer*:* None

Corresponding Author:

Emma Mellhammar, Division of Oncology and Pathology, Department of Clinical Sciences, Lund, Barngatan 2B, SE-221 85 Lund

Phone: +46-46-177501
Emma.Mellhammar@med.lu.se

Word count of paper: 4527

Financial support: Swedish Cancer Society, Mrs. Berta Kamprad's Foundation, Gunnar Nilsson's Foundation, and Governmental Funding of Clinical Research within the National Health Service.

Running title*:* Preclinical intratherapeutic PET

ABSTRACT

Positron emission tomography (PET) may provide important information on the therapeutic response of radiopharmaceutical therapy (RPT) during therapy. The radiation emission from the RPT radionuclide may disturb the coincidence detection and impair the image resolution. In this study, we tested the feasibility to perform intratherapeutic PET on three preclinical PET systems. **Methods**: Using ^{22}Na point sources and phantoms filled with ^{18}F, and a phantom filled with either ^{99m}Tc or ^{177}Lu, the coincidence count rate and the spatial resolution when both a PET and a therapeutic radionuclide were present in the PET camera, were evaluated. ^{99m}Tc was used as a substitute for a generic therapeutic radioisotope, since it has a suitable half-life and is easy obtainable. **Results**: High activities of ^{99m}Tc deteriorated the coincidence count rate from the ^{18}F-filled phantom with a ^{22}Na point source on all three systems evaluated. One of the systems could to a high degree correct the count rate with its dead time correction. The spatial resolution was degraded at high activities of ^{99m}Tc for all systems. On one of the systems ^{177}Lu increased the coincidence count rate and slightly affected the spatial resolution. The results for high activities of ^{177}Lu were similar to those for ^{99m}Tc. **Conclusion**: Intratherapeutic imaging might be a feasible method to study RPT treatment response. However, some sensitive preclinical PET systems, unable to handle high count rates, suffer count losses and may also introduce image artifacts.

Key words: PET, Radionuclide therapy, Dead time, Pile up, Image distortion

INTRODUCTION

The use of RPT to treat cancer has advanced in the last decades with introduction of more effective targeting molecules (*1*). Today high activities of radionuclides or radionuclide labelled molecules are used clinically to treat e.g. thyroid cancer (*2*), lymphomas (*3,4*), and neuroendocrine tumors (*5*). Hopes of expanding the field has grown by the development of effective labeling methods for e.g. antibodies, peptides and affibodies, to therapeutic radionuclides (*6-8*). In the development of these compounds, better tools measuring the therapeutic response in the tumor tissue in vivo are needed.

Intratherapeutic imaging, i.e. simultaneous PET during RPT, would be of interest to perform early evaluation of the therapeutic effect. In preclinical studies of therapeutic radiopharmaceuticals, longitudinal data collected throughout the treatment would reduce the need to sacrifice many animals of the model used. Intratherapeutic imaging could enhance the understanding of treatment response, offering other biomarkers to be used such as for perfusion and hypoxia, to compliment tumor size variations, which is the standard evaluation metric in vivo.

Many of the radionuclides used for therapy emit not only radiation desirable for treatment, such as α- or β-particles, low energy conversion and/or Auger electrons, but also photons and X-rays. Some of these have energies high enough to penetrate the body of a patient or animal. This can be very useful when performing biodistribution measurements and dosimetry calculations. To study therapeutic effects related to the uptake of the therapeutic radiopharmaceutical and absorbed dose and dose rate, it would be desirable to use a diagnostic radiopharmaceutical simultaneously.

PET is a common method of molecular imaging, detecting the uptake of positron emitting radiopharmaceuticals. One example is ^{18}F-FDG which detects the glucose distribution, and dynamic imaging and pharmacokinetics enable measurement of tumor blood perfusion and metabolism over time. In preclinical studies such studies could further increase the understanding of RPT. The complex effects of hypoxia on tumor therapy are likely to have big implications on the design of treatment protocols and can be evaluated with a

number of PET radiopharmaceuticals, including e.g. ^{18}F-MISO (*9*). PET also provides, among others, tracers for angiogenesis (*10*), tumor cell proliferation and apoptosis (*11*).

When applying PET for intratherapeutic imaging, there may be a risk that the photon emissions from the therapeutic radiopharmaceutical will compromise the performance of the PET camera. Secondary gamma emissions, emitted from the therapeutic radionuclide can severely affect the acquisition. High photon fluence rates will perturb the detection of coincidences as the detector system will be busy with handling single events without corresponding events in an opposing detector element (i.e. decreasing detector life time).

The fast coincidence data acquisition and processing in modern clinical and preclinical PET-systems can sort out single events detected that do not originate from an annihilation event or which have been scattered and lost energy. To allow detection of annihilation photons, even if they do not deposit their full energy in the detector, and to allow small angle scattered annihilation photons to contribute to the count rate, a wide energy window is set somewhere between 100-700 keV.

All photons interacting in the detector will occupy a part of the available time ("live period") it takes the system to process the event. Therefore, all events, including those that do not originate from an annihilation of a positron, increase the total count rate. At high count rates, due to dead time and pile-up effects, the number of detected coincidences can be compromised. Depending on the dead time characteristics of the system, events are lost in the time interval when the system is occupied processing a previous event. Pile-up can both add and subtract events from the final number of coincidences detected. Two photons may, if piled up, fall within the energy window and therefore add to the number of detected events. Similarly, photons detected inside the energy window may be "pushed over" the upper energy level if piled up with a photon of sufficient but lower energy. Therefore pile-up both reduces the statistical quality of the image and can cause miss-positioning of true coincidence events (*12*).

The influence of a therapeutic radiopharmaceutical on a PET acquisition will depend on the activity, the photon or x-ray yield (Bremsstrahlung can be neglected) and the energy of the emitted photons.

In this study, we aimed to investigate the impact of intratherapeutic imaging on the performance of three different preclinical PET cameras. The coincidence count rate and spatial resolution were investigated when high activities of therapeutic radionuclides were present in the field of view (FOV) during PET acquisition. We report that intratherapeutic imaging is feasible below certain activities and photon fluence rates on some preclinical PET systems.

MATERIALS AND METHODS

PET systems

Three different preclinical PET systems were evaluated for intratherapeutical imaging. For two of them, the Inveon (Siemens Medical Solutions, Inc) and NanoPET/CT (BioScan Inc., manufactured by Mediso) the detectors are assembled in a ring geometry, while for the third system Genisys4 (Sofie BioSciences), four detector blocks are set up as a box. The Siemens and Sofie BioSciences systems were located at University of California, Los Angeles (UCLA) whereas the BioScan system was located at Lund University Bioimaging Center. These systems characteristics have been published elsewhere (*13-16*) and their main characteristics are summarized in Table 1.

The data for all systems were reconstructed in 5 minutes frames with the manufacturers recommended algorithms, Maximum Likelihood Expectation Maximization (60 iterations) for Genisys4, Ordered Subset Expectation Maximization (18 iterations, 16 subsets) for Inveon and Ordered Subset Expectation Maximization 2D (5 subsets, 6 iterations) for NanoPET/CT.

The three PET systems evaluated all differ in presentation of count rate data and the user availability. These are commercial systems designed to be user friendly and perform the data analysis in the background, only presenting the relevant results to the user. On the Inveon and Genisys4 both true, prompt and random coincidences are retrievable from the files created during the data acquisition (header-file and list-mode file). On the NanoPET/CT system the coincidence rate and singles rate for each detector module is recorded each second in the list-mode file and an associated “events rates file”. The coincidence rate is assumed to be the prompt coincidences, i.e. with the random prompts included.

Count rate measurements

Three different high count rate measurements were performed using decaying sources and phantoms as summarized in Table 2. To imitate a therapeutic radionuclide in the Field-of-View (FOV) of the PET system, emitting photons in the same energy range as for ^{177}Lu used for therapy, ^{99m}Tc was introduced as a surrogate.

Count rate capability with ^{18}F source (Study 1). This study was performed to study the count rate capability of each PET system. A ^{18}F-source was measured throughout its decay for several hours.

Count rate capability with ^{22}Na source and ^{99m}Tc-background (Study 2a). This measurement followed the decay of ^{99m}Tc in an in-house made mouse phantom, seen in Figure 1. In its middle channel a point source of ^{22}Na was placed. The half-life of ^{22}Na ($T_{/2}$: 2.6 y) is very long compared to ^{99m}Tc ($T_{/2}$: 6.02 h) and can be considered as a constant activity and the annihilation rate due to it will not change for the duration of the measurement. The changes in coincidences count rate were then due to the influence of the photon fluence rate and decay of ^{99m}Tc.

Random coincidences from ^{99m}Tc-background on NanoPET/CT system (Study 2b). To get a measurement of random coincidences generated on the NanoPET/CT system, a ^{99m}Tc-filled phantom was measured alone. All coincidences detected will then be random. The true coincidence count rate in study 2a could be reviled by subtracting the coincidence count rate in study 2b.

Count rate capability with ^{22}Na source and ^{177}Lu-background (Study 2c). The study was performed like study 2a but the ^{99m}Tc was replaced by ^{177}Lu, a therapeutic radionuclide used for RPT.

Count rate capability with ^{18}F source together with ^{99m}Tc background (Study 3). This study was performed to study the changes in count rate seen in study 1 on each PET system due to a background emission of photons from ^{99m}Tc. A ^{18}F-source was measured throughout its decay for several hours with ^{99m}Tc alongside the ^{18}F.

Phantoms

Three forms of phantoms were used in the studies, spherical hollow phantoms (Hollow Sphere Sets (6)™, Data Spectrum) of volumes 0.5 and 1.0 mL, a NEMA NU 4-2008 ^{TM} (Data Spectrum) mouse phantom and an in-house made mouse phantom made of epoxy resin with silicon tubes to be filled with activity as seen on Figure

1. In the NEMA phantom the two fillable chambers of volume 0.7 mL were used. The mouse phantom measure 90x30x20 mm^3 and have five channels drilled at distances from surface of 0, 2.5, 5.0 7.5 and 10.0 mm as seen in Figure 1. The silicon tube has an inner diameter of 0.8 mm. For studies performed on the NanoPET/CT system, the point source used was too large to be put inside the channels. It was therefore placed on top of the phantom, see Figure 1. The use of the phantoms with the different combinations of radionuclides is described in Table 2.

Radioactivity

^{177}Lu was purchased from IDB Holland. ^{99m}Tc was obtained from a ^{99}Mo/^{99m}Tc generator and ^{18}F was produced at the Cyclotron unit at Skåne University Hospital in Lund. For studies at UCLA, ^{99m}Tc was obtained from Triad Isotopes Inc., and ^{18}F was obtained from the Biomedical Cyclotron Facility at UCLA. The main characteristics for the radionuclides used are summarized in Table 3.

Spatial resolution/Image quality

To study the effect on the spatial resolution of the reconstructed images from study 2a and 2c the Full Width at Half Maximum and Full Width at Tenth Maximum was calculated for a line profile over the ^{22}Na source. The volume resolution was calculated as the product of the Full Width at Half Maximum or Full Width at Tenth Maximum in the x,y and z directions of the image data.

RESULTS

Count rate capability with ^{18}F source

Phantom studies revealed the count rate characteristics of the three PET systems evaluated and the coincidence count rate performances found are shown in Figure 2. For activities up to 1.6 MBq of ^{18}F, the single and coincidence count rate on the Genisys4 system steadily increased, but for higher activities quickly dropped off due to a high paralyzing dead time. The NanoPET/CT and Inveon detectors accept higher activities and could handle higher count rates before dead time lead to paralysis. The Inveon reached its maximum coincidence count rate at 185 MBq of ^{18}F. Similarly the NanoPET/CT reach its maximum count rate at 54 MBq of ^{18}F.

Count rate capability with ^{22}Na source and ^{99m}Tc-background

The initial high activity of ^{99m}Tc placed in the PET system together with the ^{22}Na point source of 74 kBq affected the coincidence count rate detected for all three systems, Figure 3A-C. The Genisys4 system was continuously losing true coincidence counts for increasing activities of ^{99m}Tc in the interval examined (29 MBq – 0.2 MBq). The amounts of random coincidences notably increased between 1 and 8 MBq ^{99m}Tc. At even higher activities, all detected coincidences quickly decreased due to dead time paralysis.

For the Inveon system (Fig. 3B) the activity in the initial time frame was 500 MBq of ^{99m}Tc present in the FOV together with the point source of ^{22}Na at 74 kBq. This reduced the detected true coincidence rate to about a third of the true coincidence count rate without ^{99m}Tc activity present. The number of coincidences was constant for activities up to about 10 MBq. For activities over 50 MBq the number of detected coincidences fell off approximately exponentially with increased ^{99m}Tc activity. Random coincidences remained negligible up to 250 MBq of ^{99m}Tc, where an increase was noticed. Correcting the true coincidence rate with the dead-time correction factor available on the Inveon system, compensated for the coincidence count rate losses seen at ^{99m}Tc activities over 50 MBq.

On the NanoPET/CT system the total coincidence rate was constant up to about 5 MBq of ^{99m}Tc and then increased to a maximum at 175 MBq (Fig. 3C).

The spatial resolution evaluated was found to be degraded when high ^{99m}Tc activity was present with the ^{22}Na point source (Fig. 4A-C). The Full Width at Half Maximum was broadened by 20 % at 1.8, 115 and 110 MBq ^{99m}Tc for the Genisys4, Inveon and NanoPET/CT system respectively.

Random coincidences from ^{99m}Tc-background on NanoPET/CT system

To verify that the increased count rate in study 2a on the NanoPET/CT system was due to random coincidences, 500 MBq of ^{99m}Tc was imaged alone. The coincidence count rate, plotted as randoms in Figure 3C, followed the same trajectory as seen in study 2a, though this time rising to the maximum count rate from a baseline of almost zero coincidences detected for activities below 5 MBq, reaching its maximum count rate at approximately the same activity as in study 2a, 175 MBq. The true coincidence count rate calculated is also plotted in Figure 3C.

Count rate capability with ^{22}Na source and ^{177}Lu-background

Using the therapeutic radionuclide, ^{177}Lu on the NanoPET/CT gave results similar to those found for this system with ^{99m}Tc. At activities higher than 10 MBq ^{177}Lu the count rate increased quickly, seen in Figure 3C. The maximum activity used, 88 MBq did not clearly affect the spatial resolution (Fig. 4C). The main gamma emission for ^{99m}Tc at 140 keV has a photon yield of 89 %, and the most prominent gamma emissions from ^{177}Lu at 113 keV and 208 keV each have a photon yield of 6.4 % and 11.0 %. Assuming these all interact in the detectors with the same probability, we need roughly 5 times the activity of ^{177}Lu to have the same photon fluence rate as ^{99m}Tc.

Count rate capability with ^{18}F source together with ^{99m}Tc background

Comparisons of the count rate with and without ^{99m}Tc are found in Figure 5A-C, for each system respectively. The introduction of ^{99m}Tc in the FOV resulted in coincidence count rates diverging from those found for ^{18}F alone. The initial activities of ^{99m}Tc disrupted the count rate for all systems. As both the ^{18}F and ^{99m}Tc decay, the divergence was reduced. The Genisys4 and Inveon systems responded similarly to study 2a, losing coincidence counts in relation to the amount of ^{99m}Tc activity. The NanoPET/CT experienced a higher count rate loss at higher activities of the two radionuclides, due to dead time, but at lower activities measured a higher count rate from the high number of random counts.

The dead time correction factor readily available to the user on the Inveon system was able to correct the divergence as seen in Figure 5B.

DISCUSSION

To develop targeted RPT, that specifically finds and disseminates cancer cells, has been the leading strategy to find new and better treatments for cancer. Linking a ligand with radionuclides to construct a radiopharmaceutical can either be meant as the primary therapy, or might have a dual or even synergetic effect with the activation of the body's own immune system, the inhibition of cell signaling vital to the cancer cell, and the radiotherapeutic effect. For aggressive cancers that so far have been difficult to treat with poor prognosis, combined regiments of different targeted treatments might be the future. To optimize the strategies

it will be crucial to accurately quantify the therapeutic response in vivo during and after therapy. Changes in the tumor size, tumor viscosity, the extracellular microenvironment and other factors that enable and limit the tumor, can be prognostic factors and can help make decisions on further treatment. Comprehensive review can be found elsewhere (*17*).

This study has shown the feasibility to perform intratherapeutical PET-imaging on preclinical systems. The intricate data processing in the PET systems investigated, can to a varying degree handle additional high photon fluence impinging on the detector creating high count rates. In the case of the NanoPET/CT system, even activities of ^{177}Lu higher than those usually used in preclinical studies, did not seem to diminish the spatial resolution. As shown in Figure 4C the ^{99m}Tc was a good surrogate for ^{177}Lu as measured on the NanoPET/CT system (no such studies was possible at UCLA due to no ^{177}Lu license.

Using ^{99m}Tc as a surrogate for a hypothetical therapeutic radionuclide is, due to its availability at nuclear medicine clinics and its comparatively low price, a helpful method to evaluate the plausibility to perform intratherapeutic PET imaging on PET systems. ^{99m}Tc main photon emission at 140 keV is comparable to the 113 keV and 208 keV photon emission of ^{177}Lu. Approximating equal probability to interact in the detector and effect on count rate for the photon emissions, equal photon fluence should result in similar count rates and effects on the resolution. The difference in photon yield can therefore be used to approximate the activities of ^{99m}Tc and ^{177}Lu needed to cause comparable photon fluence rates.

The Genisys4 systems high sensitivity and lower count rate capabilities reduces the amount of activity that can be handled by the system, including the PET radionuclide. The system loses a linear relationship between count rate and activity at low activities, but this error could potentially fairly easily be compensated for with an accurated dead-time correction model, as demonstrated on the Inveon system (Fig. 2B). In the ^{99m}Tc activity interval investigated in Figure 3 the system never reach a constant count rate. This is however expected to happen for low enough activities. The interval was chosen to imitate a photon fluence relevant in RPT. In the case of ^{177}Lu therapy, activities of 20-40 MBq are administrated preclinically, and would probably influence the performance of the Genisys4 since the detector system is paralyzed at 10 MBq of ^{99m}Tc.

The Inveon and NanoPET/CT can handle the activity levels relevant for preclinical intratherapeutic imaging. While the Genisys4 system is limited by its dead time losses, the Inveon and NanoPET/CT may suffer more from resolution losses due to event pile up as this increases with count rate.

The spatial resolution was maintained on two of the systems up to therapeutic activities. Thus it is of importance for good image quality at high photon fluences to know the systems limitations.

The NanoPET/CT system showed an interesting higher sensitivity to produce random events from the ^{99m}Tc, as the random coincidence rate started to increase for ^{99m}Tc activities higher than 5 MBq and led to a net increase in prompt coincidence count rate up to 175 MBq. After reaching a maximum count rate the effects of dead time dominated and the count rate dropped.

CONCLUSION

A simple method has been presented to evaluate the count rate capability for preclinical PET systems executing intratherapeutical imaging. The systems evaluated showed clear dependence on impinging extra photon fluence rate affecting both count losses as well as spatial resolution. For therapy activities of 10-50 MBq of ^{177}Lu, two of the systems will start to experience coincidence count losses however with negligible losses of spatial resolution. The third investigated system was not able to handle such high activities.

DISCLOSURE

The authors have nothing to disclose.

ACKNOWLEDGMENTS

This research was supported by grants from the Swedish Cancer Society, Mrs. Berta Kamprad's Foundation, Gunnar Nilsson's Foundation, and Governmental Funding of Clinical Research within the National Health Service.

Disclosure

Nothing to disclose.

REFERENCES

1. Kramer-Marek G, Capala J. The role of nuclear medicine in modern therapy of cancer. *Tumour Biol.* 2012;33:629-640.

2. Mayson SE, Yoo DC, Gopalakrishnan G. The evolving use of radioiodine therapy in differentiated thyroid cancer. *Oncology.* 2015;88:247-256.

3. Goldsmith SJ. Radioimmunotherapy of lymphoma: Bexxar and Zevalin. *Semin Nucl Med.* 2010;40:122-135.

4. Druce MR, Lewington V, Grossman AB. Targeted radionuclide therapy for neuroendocrine tumours: principles and application. *Neuroendocrinology.* 2010;91:1-15.

5. Gulenchyn KY, Yao X, Asa SL, Singh S, Law C. Radionuclide therapy in neuroendocrine tumours: a systematic review. *Clin Oncol (R Coll Radiol).* 2012;24:294-308.

6. Larson SM, Carrasquillo JA, Cheung NK, Press OW. Radioimmunotherapy of human tumours. *Nat Rev Cancer.* 2015;15:347-360.

7. Fani M, Maecke HR. Radiopharmaceutical development of radiolabelled peptides. *Eur J Nucl Med Mol Imaging.* 2012;39 Suppl 1:S11-30.

8. Orlova A, Feldwisch J, Abrahmsén L, Tolmachev V. Update: Affibody Molecules for Molecular Imaging and Therapy for Cancer. *Cancer Biother Radiopharm.* 2007;22:573-584.

9. Rajendran JG, Krohn KA. F-18 fluoromisonidazole for imaging tumor hypoxia: imaging the microenvironment for personalized cancer therapy. *Semin Nucl Med.* 2015;45:151-162.

10. Oxboel J, Brandt-Larsen M, Schjoeth-Eskesen C, et al. Comparison of two new angiogenesis PET tracers 68Ga-NODAGA-E[c(RGDyK)]2 and (64)Cu-NODAGA-E[c(RGDyK)]2; in vivo imaging studies in human xenograft tumors. *Nucl Med Biol.* 2014;41:259-267.

11. Nguyen QD, Aboagye EO. Imaging the life and death of tumors in living subjects: Preclinical PET imaging of proliferation and apoptosis. *Integr Biol (Camb).* 2010;2:483-495.

12. Germano G, Hoffman E. A study of data loss and mispositioning due to pileup in 2-D detectors in PET. *IEEE Trans Nucl Sci.* 1990;37:671-675.

13. Szanda I, Mackewn J, Patay G, et al. National Electrical Manufacturers Association NU-4 performance evaluation of the PET component of the NanoPET/CT preclinical PET/CT scanner. *J Nucl Med.* 2011;52:1741-1747.

14. Bai B, Dahlbom M, Park R, et al. Performance Comparison of GENISYS4 and microPET Preclinical PET Scanners. *IEEE Nucl Sci Symp Conf Rec*; 2012.

15. Bao Q, Newport D, Chen M, Stout DB, Chatziioannou AF. Performance evaluation of the inveon dedicated PET preclinical tomograph based on the NEMA NU-4 standards. *J Nucl Med.* 2009;50:401-408.

16. Goertzen AL, Bao Q, Bergeron M, et al. NEMA NU 4-2008 comparison of preclinical PET imaging systems. *J Nucl Med.* 2012;53:1300-1309.

17. Vallabhajosula S. Molecular Imaging in Oncology. *Molecular Imaging: Radiopharmaceuticals for PET and SPECT*. Berlin, Heidelberg: Springer Berlin Heidelberg; 2009:215-254.

Figure Legends

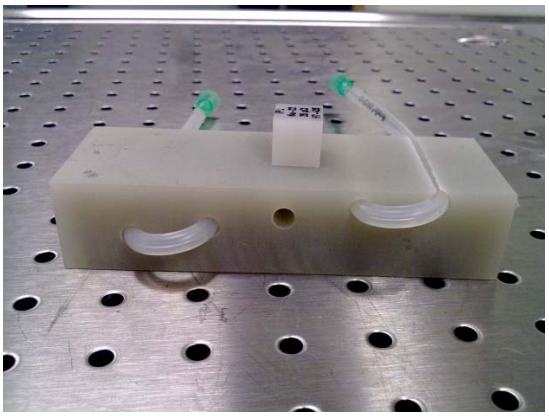

FIGURE 1. In house made mouse phantom. Epoxy harts block with 5 channels drilled at varying depths, the most shallow at the surface and the other at depths 0.25, 0.5, 0.75 and 1.0 cm. In study 2a-c and 3 a thin silicone tube is drawn through the channels. A ^{22}Na point source was placed in the middle most channel, except when used on the NanoPET/CT, where the point source encapsulated in plastic was to large, and instead placed on top of the phantom, as shown.

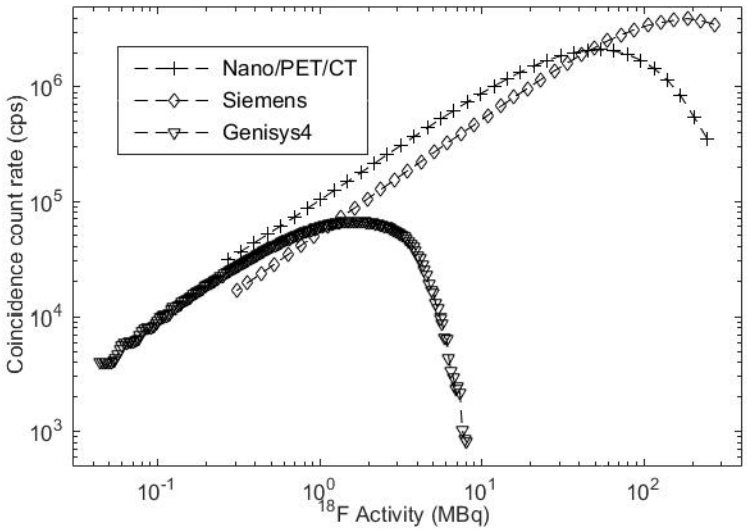

FIGURE 2. True Coincidence count rates (for Genisys4 and Inveon system, the coincidence count rate available on NanoPET) detected on the Genisys4, Inveon and NanoPET/CT when high activities of ^{18}F is allowed to decay in the PET system in study 1, as described in Table 2.

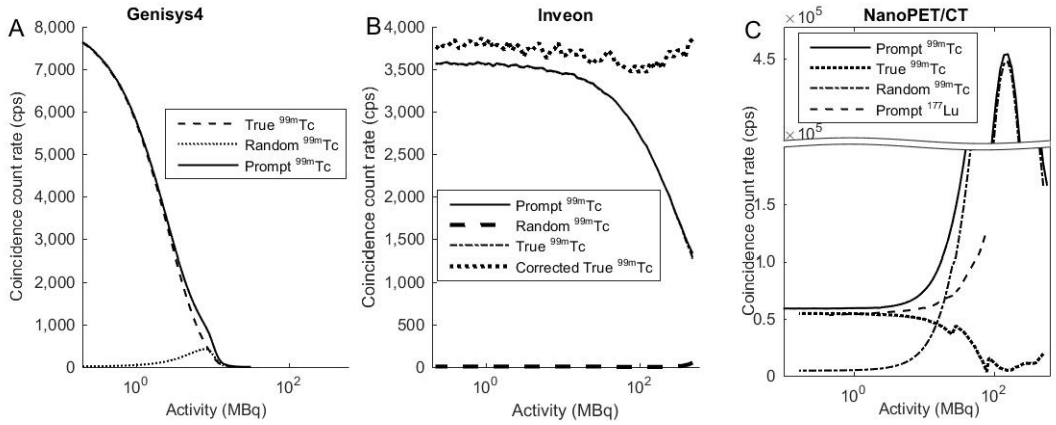

FIGURE 3. Coincidence count rates when a ^{22}Na point source is imaged together with decaying ^{99m}Tc (study 2a) for Genisys4 (A), Inveon (B) and NanoPET/CT (C). Also, correction of count rate for study 2a for Inveon in (B). In (C) also coincidence count rates for ^{99m}Tc decaying (study 2b) and ^{22}Na point source imaged together with ^{177}Lu decaying (study 2c) on the NanoPET system.

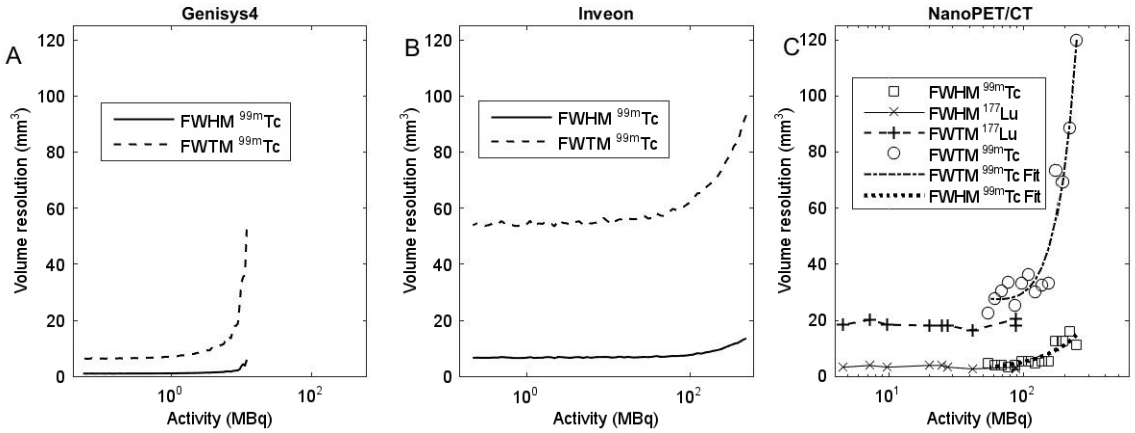

FIGURE 4. Volume resolution for Genisys4 (A), Inveon (B) and NanoPET/CT (C) measured over a ^{22}Na point source imaged together with decaying ^{99m}Tc (study 2a). Also, in (C), volume resolution measured over a ^{22}Na point source together with decaying ^{177}Lu for NanoPET/CT (study 2c).

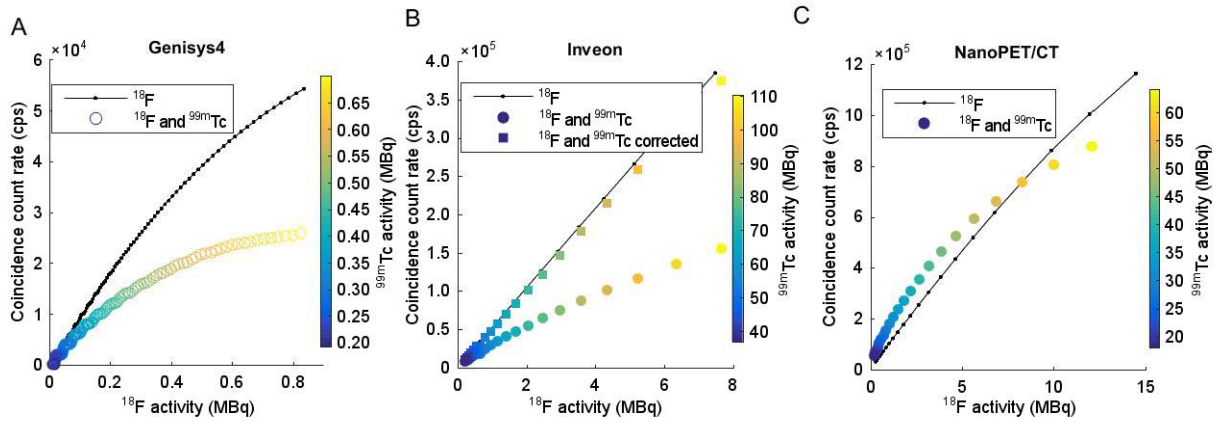

FIGURE 5. Compared true coincidence count rates detected for ^{18}F decaying alone (study 1) and together with ^{99m}Tc (study 3) on the Genisys4 (A), Inveon (B) and NanoPET/CT (C) (on NanoPET system available count rates plotted). Also, correction of count rate for study 3 plotted in (B) for the Inveon.

TABLE 1 PET system characteristics.

Characteristics	Inveon	NanoPET/CT	Genisys4
Detector material	LSO	LYSO:Ce	BGO
Crystal dimensions (mm^3)	1.5x1.5x10	1.12x1.12x 13	1.8x1.8x7
Axial FOV (mm)	127	95	94
Transaxial FOV (mm)	100	123	45
Energy window (keV)	350-650	400-600	150-650
Coincidence window (ns)	3.4	5	20
Sensitivity (%)	6.7	7.7	14
Image spatial resolution (mm)	1.8	1	1.4
Energy resolution (511 keV) (%)	14.6%	19 %	18.0%
Crystal decay time (ns)	47	41	300
Number of detectors	64	12	4
Number of crystals per detector	400	1200	3159

TABLE 2 Specific activities and phantoms used.

Study name	Radio nuclide(s)	Phantom(s)	Activity Inveon (MBq)	Activity Genisys4 (MBq)	Activity NanoPET/CT (MBq)
1	^{18}F	Sphere phantom/NEMA NU 4*	^{18}F: 270	^{18}F: 11	^{18}F: 250
2a	^{22}Na , ^{99m}Tc	Point source and block phantom†	^{99m}Tc: 500 ^{22}Na: 0.074	^{99m}Tc:170 ^{22}Na: 0.074	^{99m}Tc: 550 ^{22}Na: 0.43
2b	^{99m}Tc	Sphere phantom	-	-	^{99m}Tc: 480
2c	^{22}Na and ^{177}Lu	Point source and block phantom‡	-	-	^{177}Lu:82 ^{22}Na: 0.43
3	^{18}F , ^{99m}Tc	Sphere phantoms/ NEMA NU 4§	^{18}F: 7.7 ^{99m}Tc:110	^{18}F: 0.85 ^{99m}Tc: 0.71	^{18}F:12 ^{99m}Tc: 64

* 0.5 mL sphere phantom for ^{18}F.

† ^{22}Na point souce placed in middle channel, silicon tube pulled through the surrounding four channels.

‡ ^{22}Na point souce placed in middle channel, silicon tube pulled through the surrounding four channels.

§ 1.0 mL sphere for ^{99m}Tc and 0.5 mL for ^{18}F.

TABLE 3 Radionuclides used in this report.

Isotope	Half-life**	Decay mode	Q-value (keV)	Branching (%)	Gammas (keV)	Gamma yield (%)
^{177}**Lu**	6.734 d	β^-	498.3	100	113 208	6.4 11.0
^{18}**F**	109.77 m	e, β^+	1655.5 633.5	3.27 96.73	-	-
^{99m}**Tc**	6.01 h	IT	-	100	140.511 142.628	89 0.0187
^{22}**Na**	2.6019 y	e, β^+	2842.2	100	1274.53	99.944

** M=minutes, h=hours, d=days, y=years.